Journal of Molecular Structure 1200 (2020) 127135

Contents lists available at ScienceDirect

Journal of Molecular Structure

journal homepage: http://www.elsevier.com/locate/molstruc

The color, photophysical and electrochemical properties of azo-imine ligands and their copper(II) and platinium(II) complexes

Sultan Onur, Seyit Ali Güngör, Ferhan Tümer, Mehmet Tümer*

Chemistry Department, K.Maras Sütcü Imam University, 46100, K.Maras, Turkey

ARTICLE INFO

Article history:
Received 24 April 2019
Received in revised form
20 September 2019
Accepted 25 September 2019
Available online 26 September 2019

Keywords:
Azo-imine
Dyeing
Electrochemistry
Color
Red emission

ABSTRACT

Five novel imine based organic ligands (HL^1-HL^5) and their Cu^{2+} and Pt^{2+} metal complexes have obtained and characterized by the micro-analyses, $^1H(^{13}C)$NMR, Uv−Vis absorption, emission-excitation (PL), FT-IR and mass spectral techniques. The absorption and PL spectra for all compounds have been studied in both solution and solvent free. Results obtained from the PL spectral values of azo-imine ligands and their metal complexes have shown that there is a shift from the green band to the red band depending on the position of the OH groups and especially for the Pt^{2+} complexes. The ^{1}HNMR spectra of some of the Pt^{2+} complexes were also recorded. The results of the micro-analytic and spectroscopic methods disclosed that the metal ions coordinates to the ligands *via* the nitrogen and oxygen atoms of the azomethine and phenolic hydroxy groups. The dyeing properties of the disperse black 9 (DB9), the ligands (HL^1-HL^5) and their complexes (Cu^{2+} and Pt^{2+}) have been evaluated in terms of their dyeing behaviour on the wool fabric. The dyed wool fabrics exhibit very well to excellent washing fastness properties. However, they do not have good dyeing properties without mordant. In dyeing process, the amino edge of the wool interacts with the hydrophilic imino diethanol edges of the dyes. The Commission International de l'Eclairage (CIE) chromaticity coordinates are adjacent to the National Television Standard Committee (NTSC) standard value for red color.

1. Introduction

The obtaining of the Schiff bases is one of the easiest reactions in organic chemistry. These ligands are obtained from the condensation reactions of primary amines with a carbonyl compound such as aldehyde and/or ketone and they are colored compounds [1–4]. Schiff bases can coordinate to the transition and internal transition metal ions and consequently transition metal complexes can be obtainable. Schiff base compounds and their metal complexes have tested in the several fields such as, antimicrobial [5], anticancer [6], antimalarial [7], catalysis [8], metal ion separation [9], chemosensor [10].

Disperse Black 9 {2,2′-[4-(4-aminophenylazo)phenylimino] diethanol} is more soluble in organic solvents than in water. When disperse black 9 was used at very low concentrations in hair dyes, it is nontoxic [11]. This dye is a monoazo organic compound containing the amine group and when the primary amine group in this compound react with carbonyl compounds (ketone or aldehyde), the azo-imine ligands are obtained. It is hydrophilic in nature. DB9 is almost insoluble in water and soluble in the organic solvents. DB9 has the hydrophilic imino diethanol edges. This dye is manufactured from the diazo-reaction of the p-nitroaniline and N-phenyldiethanolamine as commercially. Although the ligands HL^1-HL^5 have the functional groups (such as OH and OCH_3) on the salicylidene ring, the ligands interact with the wool fabric *via* hydrophilic edges. Azo-imine compounds can be used in the biological and chemical many fields as a reactant or material [12–15]. Since the azo dyes have different colors such as, red, orange, brown or yellow, they can used in the textile, plastics, paint or paper industries [16–18]. As the azo-imine ligands have electron donor atoms such as oxygen and nitrogen, they interact easily with transition metal ions in the solution media and the metal complexes form.

In this paper, five azo-imine ligands [2,2'-((4-((3-hydroxy salicylidene imino)phenyl)azo)phenyl)imino)bis(ethanol) (HL^1), 2,2'-((4-((4- hydroxy salicylidene imino)phenyl)azo)phenyl)imino) bis(ethanol) (HL^2), 2,2'-((4-((5-hydroxy salicylidene imino)phenyl) azo)phenyl)imino)bis(ethanol) (HL^3), 2,2'-((4-((3,4- dihydroxy salicylidene imino)phenyl)azo)phenyl)imino)bis(ethanol) (HL^4)], 2,2'-((4-((4,6- dihydroxy salicylidene imino)phenyl)azo)phenyl)imino) bis(ethanol) (HL^5)] and their copper(II) and platinium(II) transition

* Corresponding author.
E-mail address: mtumer@ksu.edu.tr (M. Tümer).

https://doi.org/10.1016/j.molstruc.2019.127135
0022-2860/

metal complexes have been synthesized and characterized using the micro-analyses, mass spectra, FTIR, UV−vis (solution and solvent free), emission-excitation and $^{1}H(^{13}C)$NMR spectra. Additionally, electrochemical and thermal properties of the metal free ligands and their Cu^{2+} and Pt^{2+} complexes have viewed. Dyeing properties of the DB9, ligands and their metal complexes on the wool have been investigated with/without mordants. Without mordant in the dyeing process, none of DB9 and other materials have good dyeing properties on wool.

2. Methods and materials

Physical measurements have given in the Supplemantary file. In addition, dyeing procedure of the wool has also given in the Supplemantary file.

2.1. Preparation of the azo imine compounds (HL^1-HL^5)

The salicylaldehyde derivatives (1 mmol; 152 mg 3-, 4- and 5-methoxy salicylaldehyde for the ligands HL^1-HL^3) in methanol (20 mL, absolute) and the azo amine compound (Disperse Black 9) (1 mmol, 300 mg) in methanol (20 mL, absolute) were mixed and refluxed for about two days at 80 °C. The color of the solution changed to orange. After cooling the solution, the resulting precipitate was filtered and washed with cold methanol. Single crystals of the Schiff base compounds (HL^1-HL^3) suitable for X-ray diffraction study were obtained by slow evaporation of the compounds in methanol. Physical properties and other spectroscopic data are given below.

HL^1: ($C_{23}H_{24}N_4O_4$). Yield: 80%, color: dark orange, melting point: 205 °C. Elemental analyses, found (calcd. %): C, 65.79 (65.70); H, 5.82 (5.75); N, 13.25 (13.33). ^{1}H NMR ($CDCl_3$, δ (ppm)): 8.77 (s, 1H, CH═N), 7.80−6.37 (m, 11H, Ar−H), 3.70 (t, 2H, O−CH_2), 3.58 (t, 2H, N−CH_2). ^{13}C NMR ($CDCl_3$, δ (ppm)): 164.35 (CH═N), 155.20−108.70 (Ar−C), 58.10 (O−CH_2), 53.15 (N−CH_2). Mass spectrum (ESI/MS, m/z): Calcd.: 420.46, found: 421.19 $[M]^+$; calcd.: 421.46, found: 422.19 $[M+1]^+$. FT-IR: (KBr, cm^{-1}): 3336 ν(-O-H)$_{phenolic}$, 3168 ν(-O-H)$_{alph}$, 2960 ν(-C-H)$_{alph}$, 1610 ν(-CH═N-), 1506 ν(-N═N-), 1435 ν(-C-OH)$_{phenolic}$.

HL^2: ($C_{23}H_{24}N_4O_4$). Yield: 83%, color: dark orange, melting point: 203 °C. Elemental analyses, found (calcd. %): C, 65.77 (65.70); H, 5.71 (5.75); N, 13.42 (13.33). ^{1}H NMR ($CDCl_3$, δ (ppm)): 9.70 (s, 2H, Ph-OH), 8.73 (s, 1H, CH═N), 7.87−6.26 (m, 11H, Ar−H), 3.78 (t, 2H, O−CH_2), 3.67 (t, 2H, N−CH_2). ^{13}C NMR ($CDCl_3$, δ (ppm)): 165.10 (CH═N), 157.33−108.22 (Ar−C), 58.40 (O−CH_2), 53.15 (N−CH_2). Mass spectrum (ESI/MS, m/z): Calcd.: 420.46, found: 421.19 $[M]^+$; calcd.: 421.46, found: 422.19 $[M+1]^+$; calcd.: 419.45, found: 419.27 $[M-1]^+$. FT-IR: (KBr, cm^{-1}): 3225 ν(-O-H)$_{phenolic}$, 3150 ν(-O-H)$_{alph}$, 2955 ν(-C-H)$_{alph}$, 1613 ν(-CH═N-), 1508 ν(-N═N-), 1460 ν(-C-OH)$_{phenolic}$.

HL^3: ($C_{23}H_{24}N_4O_4$). Yield: 85%, color: orange, melting point: 202 °C. Elemental analyses, found (calcd. %): C, 65.76 (65.70); H, 5.68 (5.75); N, 13.41 (13.33). ^{1}H NMR ($CDCl_3$, δ (ppm)): 8.78 (s, 1H, CH═N), 7.88−6.82 (m, 11H, Ar−H), 3.79 (t, 2H, O−CH_2), 3.67 (t, 2H, N−CH_2). ^{13}C NMR ($CDCl_3$, δ (ppm)): 165.04 (CH═N), 155.50−108.65 (Ar−C), 60.45 (O−CH_2), 55.00 (N−CH_2). Mass spectrum (ESI/MS, m/z): Calcd.: 420.46, found: 421.20 $[M]^+$; calcd.: 421.46, found: 422.20 $[M+1]^+$; calcd.: 419.45, found: 419.25 $[M-1]^+$. FT-IR: (KBr, cm^{-1}): 3250 ν(-O-H)$_{phenolic}$, 3074 ν(-O-H)$_{alph}$, 2891 ν(-C-H)$_{alph}$, 1627 ν(-CH═N-), 1514 ν(-N═N-), 1467 ν(-C-OH)$_{phenolic}$.

HL^4: ($C_{23}H_{24}N_4O_5$). Yield: 88%, color: dark orange, melting point: 221 °C. Elemental analyses, found (calcd. %): C, 63.37 (63.29); H, 5.60 (5.54); N, 12.77 (12.84). ^{1}H NMR ($CDCl_3$, δ (ppm)): 11.80 (s, 3H, Ph-OH), 8.62 (s, 1H, CH═N), 7.95−6.48 (m, 10H, Ar−H), 3.75 (t, 2H, O−CH_2), 3.36 (t, 2H, N−CH_2). ^{13}C NMR ($CDCl_3$, δ (ppm)): 165.20 (CH═N), 159.72−108.15 (Ar−C), 60.34 (O−CH_2), 56.40 (N−CH_2). Mass spectrum (ESI/MS, m/z): Calcd.: 436.46, found: 436.18 $[M]^+$; calcd.: 437.46, found: 437.18 $[M+1]^+$; calcd.: 438.47, found: 438.48 $[M+1]^+$; calcd.: 439.48, found: 439.18 $[M+1]^+$. FT-IR: (KBr, cm^{-1}): 3305 ν(-O-H)$_{phenolic}$, 3219 ν(-O-H)$_{alph}$, 2965 ν(-C-H)$_{alph}$, 1599 ν(-CH═N-), 1505 ν(-N═N-), 1392 ν(-C-OH)$_{phenolic}$.

HL^5: ($C_{23}H_{24}N_4O_5$). Yield: 82%, color: dark brown, melting point: >250 °C. Elemental analyses, found (calcd. %): C, 63.21 (63.29); H, 5.47 (5.54); N, 12.90 (12.84). ^{1}H NMR ($CDCl_3$, δ (ppm)): 8.60 (s, 1H, CH═N), 7.91−6.52 (m, 10H, Ar−H), 3.94 (t, 2H, O−CH_2), 3.68 (t, 2H, N−CH_2). ^{13}C NMR ($CDCl_3$, δ (ppm)): 165.83 (CH═N), 157.50−107.45 (Ar−C), 58.12 (O−CH_2), 54.30 (N−CH_2). Mass spectrum (ESI/MS, m/z): Calcd.: 437.46, found: 437.24 $[M+1]^+$; calcd.: 410.42, found: 410.17 $[C_{21}H_{22}N_4O_5-C_2H_2]^+$; calcd.: 394.40, found: 394.19 $[C_{21}H_{20}N_3O_5\text{-}(NC_2H_4]^+$. FT-IR: (KBr, cm^{-1}): 3300 ν(-O-H)$_{phenolic}$, 3175 ν(-O-H)$_{alph}$, 2878 ν(-C-H)$_{alph}$, 1610 ν(-CH═N-), 1505 ν(-N═N-), 1443 ν(-C-OH)$_{phenolic}$.

2.2. Preparation of the Cu(II) and Pt(II) metal complexes

The complexes were prepared according to a known procedure. The azo imine ligands HL^1-HL^3 (0.434 g, 1 mmol) were dissolved in the ethanol (20 mL) solution and the metal salts [1 mmol; 0.171 g for $CuCl_2\cdot 2H_2O$; 0.420 g for $K_2[Pt(Cl)_4]$ were added to the mixture of CH_3OH (20 mL) and the solution was refluxed during 24 h. The color of the reaction solution changed to the brown or purple. The mixture was cooled to the room temperature, and the precipitated complex was filtered by vacuum, washed three times by the ethanol, and then dried under vacuum desiccator. Purity of the complexes were checked by t.l.c. studies.

$[Cu(L^1)Cl(H_2O)]3H_2O$: Yield: 65%, color: Brown, melting point: >250 °C. Elemental analyses, found (calcd. %): C, 46.22 (46.78); H, 5.18 (5.29); N, 9.44 (9.49). Mass spectrum (ESI/MS, m/z): Calcd.: 554.48, found: 555.24 $[M+H_2O]^+$, calcd.: 555.49, found: 556.24 $[M+H+H_2O]^+$, calcd.: 556.49, found: 557.25 $[M+2H + H_2O]^+$, calcd.: 510.43, found: 511.24 $[C_{21}H_{23}ClCuN_4O_5-C_2H_3OH]^+$. FT-IR: (KBr, cm^{-1}): 3433 ν(−CH_2−OH), 2925 ν(-C-H)$_{alph}$, 1598 ν(-CH═N-), 1514 ν(-N═N-), 1380 ν(-C-OH).

$[Cu(L^2)Cl(H_2O)]3H_2O$: Yield: 68%, color: Brown, melting point: >250 °C. Elemental analyses, found (calcd. %): C, 47.53 (46.78); H, 5.38 (5.29); N, 12.93 (9.49). Mass spectrum (ESI/MS, m/z): Calcd.: 536.47, found: 536.22 $[M]^+$; calcd.: 537.47, found: 538.29 $[M+1]^+$, calcd.: 554.48, found: 554.27 $[M+H_2O]^+$; calcd.: 568.50, found: 568.20 $[MCH_3OH]^+$. FT-IR: (KBr, cm^{-1}): 3434 ν(-O-H), 2925 ν(-C-H)$_{alph}$, 1598 ν(-CH═N-), 1515 ν(-N═N-), 1386 ν(-C-O).

$[Cu(L^3)Cl(H_2O)]3H_2O$: Yield: 62%, color: Brown, melting point: >250 °C. Elemental analyses, found (calcd. %): C, 46.52 (46.78); H, 5.69 (5.29); N, 9.93 (9.49). Mass spectrum (ESI/MS, m/z): Calcd.: 553.47, found: 553.24 $[M-1]^+$; calcd.: 554.48, found: 554.45 $[M+1]^+$, calcd.: 585.51, found: 584.49 $[M+H_2O+CH_3OH+1]^+$. FT-IR: (KBr, cm^{-1}): 3433 ν(-O-H), 2925 ν(-C-H)$_{alph}$, 1599 ν(-CH═N-), 1513 ν(-N═N-), 134 ν(-C-O).

$[Cu_2(L^4)Cl(H_2O)_2]$: Yield: 60%, color: Brown, melting point: >250 °C. Elemental analyses, found (calcd. %): C, 44.89 (43.71); H, 3.71 (3.99); N, 9.46 (8.86). Mass spectrum (ESI/MS, m/z): Calcd.: 633.01, found: 633.23 $[M+1]^+$; calcd.: 652.04, found: 652.25 $[M+H_2O+1]^+$. FT-IR: (KBr, cm^{-1}): 3435 ν(-O-H), 2925 ν(-C-H)$_{alph}$, 1630 ν(-CH═N-), 1506 ν(-N═N-), 1429 ν(-C-OH).

$[Cu_2(L^5)Cl(H_2O)_3]$: Yield: 63%, color: Brown, melting point: >250 °C. Elemental analyses, found (calcd. %): C, 42.58 (42.50); H, 4.27 (4.19); N, 8.70 (8.62). Mass spectrum (ESI/MS, m/z): Calcd.: 589.97, found: 590.64 $[M-C_2H_2O]^+$; calcd.: 605.97, found: 605.39 $[M-C_2H_2]^+$; calcd.: 633.01, found: 633.12 $[M+1]^+$. FT-IR: (KBr, cm^{-1}): 3440 ν(-O-H), 2971 ν(-C-H)$_{alph}$, 1631 ν(-CH═N-), 1505 ν(-N═N-), 1310 ν(-C-OH).

[Pt(L^1)Cl(H_2O)$_2$]2H_2O: Yield: 64%, color: Purple, melting point:> 250 °C. Elemental analyses, found (calcd. %): C, 39.33 (39.24); H, 4.26 (4.15); N, 7.88 (7.96). Mass spectrum (MALDI-TOF, *m/z*): Calcd.: 728.033, found: 728.067 $[M + Na]^+$; calcd.: 664.981, found: 664.306 $[M-3H]^+$; calcd.: 650.998, found: 651.218 $[M-OH]^+$. FT-IR: (KBr, cm^{-1}): 3438 ν(-O-H), 2935 $\nu(\text{-C-H})_{alph}$, 1618 ν(-CH=N-), 1502 ν(-N=N-), 1383 $\nu(\text{-C-OH})_{phenolic}$.

[Pt(L^2)Cl(H_2O)$_2$]4H_2O: Yield: 60%, color: Dark purple, melting point:> 250 °C. Elemental analyses, found (calcd. %): C, 37.38 (37.33); H, 4.59 (4.49); N, 7.68 (7.57). Mass spectrum (MALDI-TOF, *m/z*): Calcd.: 665.051, found: 668.005 $[M-3H]^+$; calcd.: 686.92, found: 686.45 $[M+Na-4H]^+$; calcd.: 701.732, found: 701.006 $[M+2Na+3H-OH]^+$; calcd.: 728.076, found: 727.951 $[M+Na+K-2H]^+$; calcd.: 776.190, found: 776.614 $[M+Na+2K]^+$; calcd.: 792.179, found: 791.226 $[M+2Na+2K]^+$. FT-IR: (KBr, cm^{-1}): 3432 ν(-O-H), 2922 $\nu(\text{-C-H})_{alph}$, 1623 ν(-CH=N-), 1509 ν(-N=N-), 1387 $\nu(\text{-C-OH})_{phenolic}$.

[Pt(L^3)ClH$_2$O]5H_2O: Yield: 68%, color: Dark purple, melting point:> 250 °C. Elemental analyses, found (calcd. %): C, 36.50 (36.44); H, 4.55 (4.65); N, 7.31 (7.39). Mass spectrum (MALDI-TOF, *m/z*): Calcd.: 522.431, found: 522.442 $[C_{19}H_{11}N_4O_2Pt]^+$; calcd.: 649.99, found: 648.221 $[M-H_2O]^+$; calcd.: 665.584, found: 668.005 $[M-2H]^+$; calcd.: 686.92, found: 686.49 $[M+Na-4H]^+$; calcd.: 774.164, found: 774.144 $[M+2Na+2K-H_2O]^+$; calcd.: 791.171, found: 790.612 $[M+2Na+2K-H]^+$. FT-IR: (KBr, cm^{-1}): 3432 ν(-O-H), 2924 $\nu(\text{-C-H})_{alph}$, 1650 ν(-CH=N-), 1511 ν(-N=N-), 1387 ν(-C-O).

[Pt$_2$(L^4)Cl(H_2O)$_3$]: Yield: 65%, color: Purple, melting point:> 250 °C. Elemental analyses, found (calcd. %): C, 30.79 (30.25); H, 2.71 (2.98); N, 6.34 (6.14). Mass spectrum (MALDI-TOF, *m/z*): Calcd.: 895.088, found: 894.606 $[M]^+$; calcd.: 825.619, found: 826.297 $[M-Cl-H_2O-OH]^+$; calcd.: 665.989, found: 665.961 $[M-Pt-2H_2O]^+$. FT-IR: (KBr, cm^{-1}): 3433 ν(-O-H), 2922 $\nu(\text{-C-H})_{alph}$, 1628 ν(-CH=N-), 1509 ν(-N=N-), 1389 ν(-C-OH).

[Pt$_2$(L^5)Cl(H_2O)$_3$]: Yield: 62%, color: Purple, melting point:> 250 °C. Elemental analyses, found (calcd. %): C, 30.44 (30.25); H, 3.11 (2.98); N, 6.25 (6.14). Mass spectrum (MALDI-TOF, *m/z*): Calcd.: 913.103, found: 914, 005 $[M]^+$; calcd.: 827.058, found: 827.075 $[M-(3H_2O+2OH)]^+$; calcd.: 702.021, found: 703.134 $[M-(Pt+H_2O)]^+$; calcd.: 568.553, found: 568.381 $[M-(Pt+Cl+2H_2O+2H_2O_2)]^+$. FT-IR: (KBr, cm^{-1}): 3430 ν(-O-H), 2925 $\nu(\text{-C-H})_{alph}$, 1625 ν(-CH=N-), 1506 ν(-N=N-), 1386 ν(-C-OH).

3. Results and discussion

3.1. Characterization of the ligands and their metal complexes

In this paper, five azo-imine ligands (HL^1-HL^5) having hydroxy groups on the different positions of the aromatic rings were obtained (Fig. 1) and characterized by using micro-analytical and spectroscopic methods. To obtain the ligands, the DB9 as primary amine was used. The ligands have the amino bis (ethylene hydroxy) group on the amine ring. This group has the hydrophilic feature. As the ligands have this group, they have high solubility in the polar organic solvents like CH_3CH_2OH, CH_3OH, $CHCl_3$, C_2H_6O etc. The imine based ligands have high thermal stabilities at room temperatures and they can be stored for a long time without decomposition. The ligands have a conjugated molecular structure and they have both inductive and mesomeric electron delocalizations on the whole molecule. The hydroxy groups on the salicylidene rings donate the π-electrons to the aromatic rings by the mesomeric affect. The ligands have the C=C, CH=N and N=N chromophore groups. In addition to, there are auxochrome groups such as OH and $N(CH_2CH_2OH)_2$ on the aromatic rings. Since these azo-imine ligands having extended π-conjugation, they commonly show strong absorption properties in the visible region.

The ^{1}HNMR(^{13}C)NMR spectral properties of the ligands (HL^1-HL^5) were viewed in the $CDCl_3$ solvent and TMS as a standard. The obtained spectral data have given in the experimental section. In the ^{1}HNMR spectra of the ligands HL^2 and HL^4, the broad signals at 9.70 and 11.80 ppm can be attributed to the phenolic hydroxy protons. The singlets at 8.60–8.78 ppm range come from the protons of the azomethine (CH=N) group. The aromatic ring protons belonging to the salicylidene and azo-amine rings were shown in the 7.95–6.26 ppm range. The methylene hydroxy protons ($-(CH_2)-OH$) were shown in the 3.94–3.70 ppm range as triplet. On the other hand, triplets in the 3.67–3.36 ppm range may be ascribed to the methylene amine ($-N(CH_2)-$) protons. The aliphatic hydroxy protons $[-N(CH_2-CH_2-OH)_2]$ were shown in the 4.78–5.01 ppm range.

In the ^{13}CNMR spectra of the ligands, the azomethine carbon atoms were determined in the 165.83–164.35 ppm range. As the ligands HL^4 and HL^5 have three hydroxy groups on the salicylidene ring, the chemical shift values of the azomethine carbon atoms have been slightly shifted to the lower regions. The aromatic ring carbon atoms were shown in the 159.72–107.45 ppm range. While the carbon atom of the ($-(CH_2)-OH$) group of the ligands was shown in the 60.45–58.10 ppm range, the carbon atom of the ($-N(CH_2)-$) group is in the 56.40–53.15 ppm range.

The FTIR spectral data for the azo-imine ligands and their Cu^{2+} and Pt^{2+} complexes were investigated using KBr as a standard and obtained data were given in the experimental section. The aromatic hydroxy stretching bands ν(O–H) of the ligands were shown in the 3336-3225 cm^{-1} range and these bands were shifted to the lower regions in the spectra of the complexes. This shift shows that the *ortho*-oxygen atom on the salicylidene ring coordinated to the metal ions. On the other hand, the aliphatic hydroxy stretchings ν(O–H) are in the 3219-3074 cm^{-1} range. The very strong bands in the 1627-1599 cm^{-1} range may be assigned to the stretching ν(CH=N) of the azomethine group. This band has been shifted to lower or higher regions in the spectra of the complexes and this circumstance supports that the nitrogen atom of the azomethine group coordinated to the metal ions. The azo (N=N) and phenolic (C–OH) group bands were shown in the 1514-1505 and 1467-1392 cm^{-1} ranges, respectively.

The mass spectral properties of the ligands and their Cu^{2+} complexes were investigated by LC-MS (ESI) method. But, their Pt^{2+} complexes were viewed by the MALDI-TOF method. The MALDI-TOF spectra of the $PtL^1(H_2O)Cl$ and $Pt_2(L^5)Cl(H_2O)_2$ have been also given in Fig. 2. The spectral data of the ligands and their Cu^{2+} and Pt^{2+} complexes are given in the experimental section. The obtained data for all compounds confirm the proposed structures.

3.2. UV–vis absorption and photoluminence properties of the ligands and their metal complexes

The UV–vis absorption and PL properties of the ligands and their Cu^{2+} and Pt^{2+} complexes were investigated in DMF solution (1.0×10^{-5} M) and solvent free. The aim of investigation of the properties of the compounds at the solvent free is to determine whether the solvent effect on the electronic transitions. The UV–vis spectra of the ligands HL^1, HL^2, HL^4 and their transition metal complexes in DMF solution (1.0×10^{-3} M) and solid state have been given in Fig. 3. The obtained absorption and photoluminescence spectral data of the ligands and their metal complexes have been given in Table 1. In the solution UV–vis spectra of the ligands, the broad and strong absorption bands in the 517-440 nm range can be assigned to the n-π* transitions of the azomethine and diazo groups. The weak bands at the shorter wavelengths (230–360 nm range) come from the π-π*, δ-π* and δ-δ* transitions of the benzenoid rings. In the spectra (DMF solution) of the metal

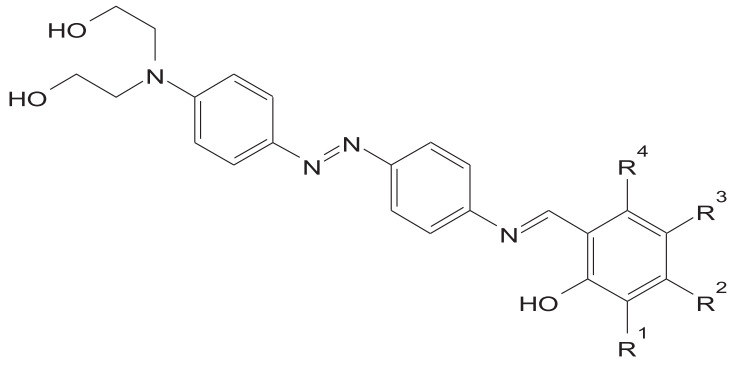

R^1: OH; R^2= R^3= R^4= H **(HL^1)**; R^2: OH; R^1= R^3= R^4= H **(HL^2)**; R^3: OH; R^1= R^2= R^4= H **(HL^3)**; R^1= R^2= OH; R^3= R^4= H **(HL^4)**; R^2= R^4= OH; R^1= R^3= H **(HL^5)**.

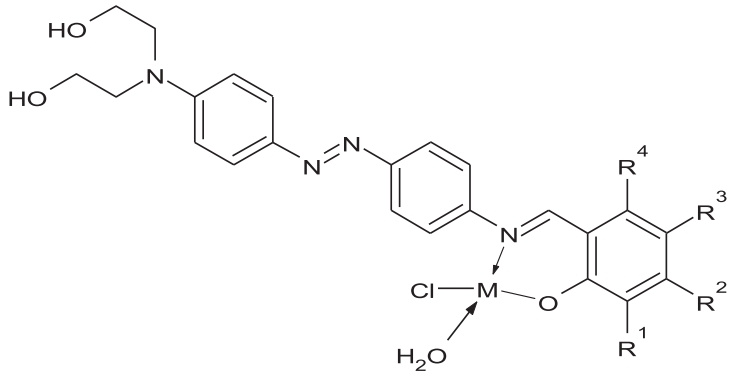

M: Cu(II), Pt(II)

Fig. 1. Proposed structures of the synthesized azo-imine ligands and their Cu^{2+} and Pt^{2+} transition metal complexes.

complexes, these bands have been shifted to the slightly shorter or longer wavelengths as a result of complexation. As the bands in the 380–550 nm range of all compounds are very broad, it is not possible to see the bands in this range in detail. But, in the spectra of some of the complexes, this band spacing has been narrowed and the electronic transitions in this range have been seen in more detail. The reason for the expansion of the band gap is that the amino bis(ethylene hydroxy) group is attached to the phenyl ring. In the spectrum of the complex $[Cu(L^2)Cl(H_2O)]3H_2O$, the weak band at 633 nm can be referred to the d-d transition of the copper(II) ion. The square-planar Pt^{2+} complexes show the d-d transitions in the 711–736 nm range. Compared to their spectra in DMF solution of the Pt^{2+} complexes, the reflectance spectral values of the Pt^{2+} complexes have shifted to the longer wavelengths. On the other hand, at the diffuse reflectance spectra of the ligands and their metal complexes, the bands in the 315-230 nm range come from the π-π*, δ-π* and δ-δ* transitions. Interestingly, while the absorption spectral data of the Cu^{2+} complexes in the DMF solution shifted to the longer wavelengths by the bathochromic effect, at the solid state, the absorbance values for the Cu^{2+} complexes have shifted to the shorter wavelengths according to the Pt^{2+} complexes.

The PL spectra of the ligands and their Cu^{2+} and Pt^{2+} complexes were studied in the DMF solution and solvent free media. The emission spectra of the HL^2 and HL^3 with their metal complexes in the DMF solution and solvent free are shown in Fig. 4. The excitation values of the ligands HL^1-HL^5 in DMF are in the 551–576 nm range. These values at the solvent free media have shifted to the shorter wavelengths (543–555 nm range). As the ligands interact with the solvent molecules in DMF solution, the excitation values have shifted to the longer wavelengths. The emission values for the

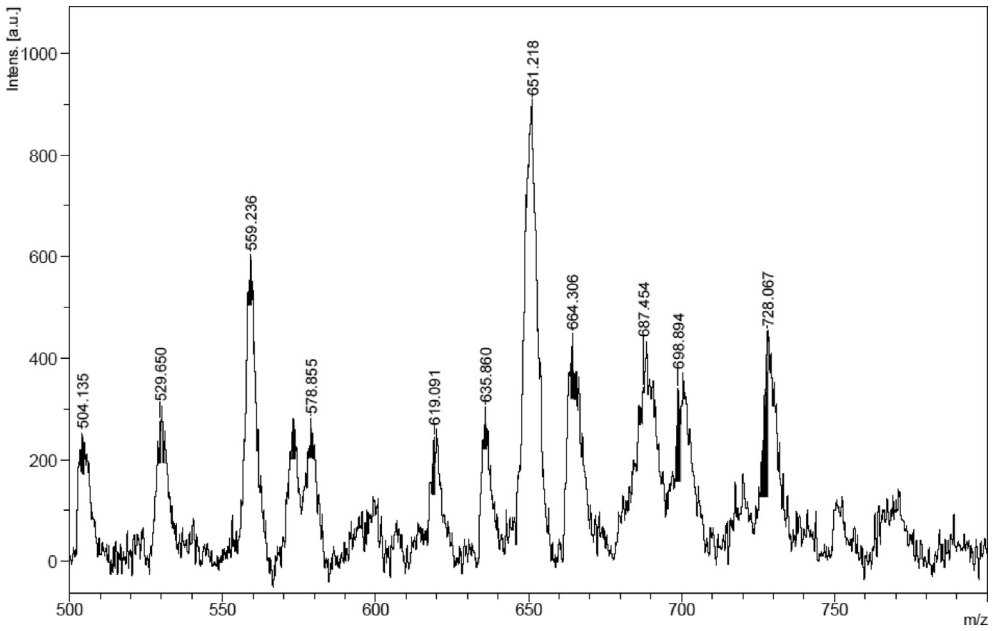

a) $PtL^1(H_2O)Cl$

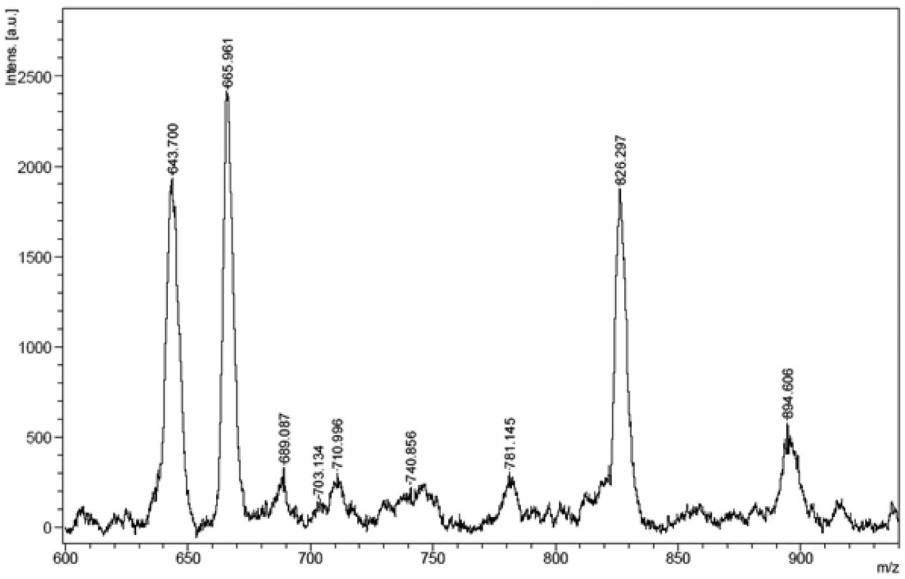

b) $Pt_2(L^5)Cl(H_2O)_2$

Fig. 2. The MALDI-TOF spectra of the Pt(II) complexes of the ligands HL^1 and HL^5.

ligands in DMF solution are in the 568−625 nm range. The emission bands of the metal-free ligand may be due to the ligand centered $\pi^* \rightarrow \pi$ transition. In the spectra of the ligands HL^2 and HL^5, there are two emission bands. On the one hand, at solvent free media, the emission values of the free ligands are shifted to the green region. The Cu^{2+} complexes have the excitation values in the 573-533 nm range in DMF solution. The excitation values at the solvent free media of the Cu^{2+} complexes have found in the 547−549 nm range. Whereas, the Pt(II) complexes have the excitation values in the 605-527 nm range in DMF solution. At the solvent free media, the Pt^{2+} complexes have excitation values in the 664-610 nm range. The emission spectra in DMF solution of the Cu^{2+} complexes of the ligands HL^1, HL^2 and HL^3 contain two peaks in the 650-570 nm range, but there is only one peak in the spectra of the other Cu^{2+} complexes. The emission values of the Pt^{2+} complexes are in the 590−648 nm range. At the solvent free media, the values of the Pt^{2+} complexes have shifted to the red emission region. When the photophysical properties of ligands and metal complexes are examined, it has been determined that the compounds have different spectral values in solvent medium and solid state. As the interaction between the solvent and the free ligands in the DMF solution is strong (as the hydrogen bonding), the PL spectral values shift to the longer wavelengths. The hydrogen bonding interaction between the free ligands and the solvent molecules is removed by the formation of complex compounds [19]. As a result, the PL values of the complexes at the solid state (especially for the Pt^{2+}

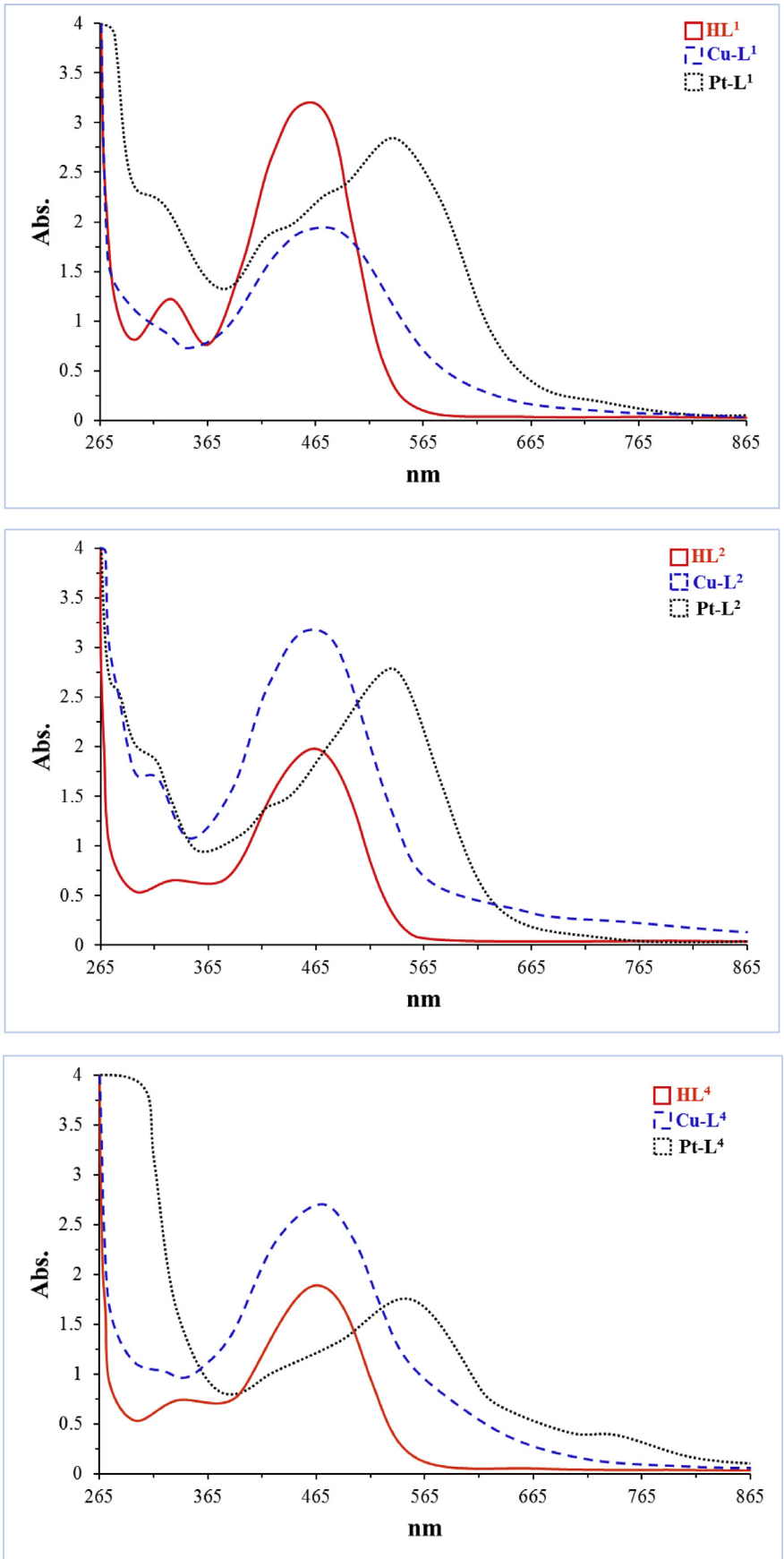

Fig. 3. The UV–vis spectra of the ligands HL^1, HL^2, HL^4 and their transition metal complexes in DMF solution (1.0×10^{-5} M).

Table 1
UV visible and photoluminescence datas of the ligands and their Cu(II), Pt(II) complexes in the 1.0×10^{-5} M DMF solution and solid state.

Compounds	(λ_{max})			
	Solution (DMF) (Solid State)			
	Excitation	Emission	λ (ϵ) Solution (DMF)	Solid State
HL^1	576 (548)	593 (569)	331(1.22×10^5), 459(3.21×10^5)	235, 332, 374, 456, 517
$[Cu(L^1)Cl(H_2O)]3H_2O$	571 (549)	588, 624 (556)	332(0.91×10^5), 476(1.94×10^5)	227, 300, 415, 528
$[Pt(L^1)Cl(H_2O)_2]2H_2O$	579 (661)	597, 631 (678)	319(2.22×10^5), 429(1.92×10^5), 471(2.26×10^5), 535(2.86×10^5), 736(0.17×10^5)	231, 316, 421, 546, 751
HL^2	551 (544)	568, 625 (565)	333(0.65×10^5), 463(1.97×10^5)	231, 329, 464
$[Cu(L^2)Cl(H_2O)]3H_2O$	552 (548)	570, 611 (570)	313(1.70×10^5), 462(3.16×10^5), 633(0.39×10^5)	231, 309, 333, 504
$[Pt(L^2)Cl(H_2O)_2]4H_2O$	576 (610)	590, 632 (630)	282(2.51×10^5), 315(1.87×10^5), 416(1.36×10^5), 535(2.79×10^5), 711(0.09×10^5)	231, 331, 409, 523, 753
HL^3	560 (555)	580 (558)	325(0.48×10^5), 468(1.44×10^5)	228, 327, 446
$[Cu(L^3)Cl(H_2O)]3H_2O$	573 (547)	591, 650 (553)	325(1.42×10^5), 466(3.32×10^5)	231, 333, 542
$[Pt(L^3)ClH_2O]5H_2O$	580 (662)	597, 638 (666)	300(1.61×10^5), 366(1.41×10^5), 433(0.96×10^5), 535(1.74×10^5), 732(0.28×10^5)	230, 311, 409, 535, 750
HL^4	568 (543)	584 (553)	337(0.73×10^5), 467(1.88×10^5)	238, 525, 416, 482
$Cu_2(L^4)Cl(H_2O)_2$	595 (547)	611 (557)	321(1.03×10^5), 468(2.70×10^5)	236, 309, 475
$[Pt_2(L^4)Cl(H_2O)_3]$	566, 605 (664)	619 (673)	424(1.01×10^5), 545(1.75×10^5), 736(0.38×10^5)	231, 321, 540, 748
HL^5	565 (544)	572, 615 (552)	327(0.67×10^5), 472(3.19×10^5), 550(1.89×10^5)	234, 279, 328, 505
$Cu_2(L^5)Cl(H_2O)_2$	533, 575 (548)	592 (555)	325(3.52×10^5), 469(1.52×10^5)	236, 307, 491
$[Pt_2(L^5)Cl(H_2O)_3]$	527, 601 (657)	618, 648 (668)	320(0.49×10^5), 380(2.03×10^5), 415(0.50×10^5), 535(1.25×10^5)	232, 309, 530, 752

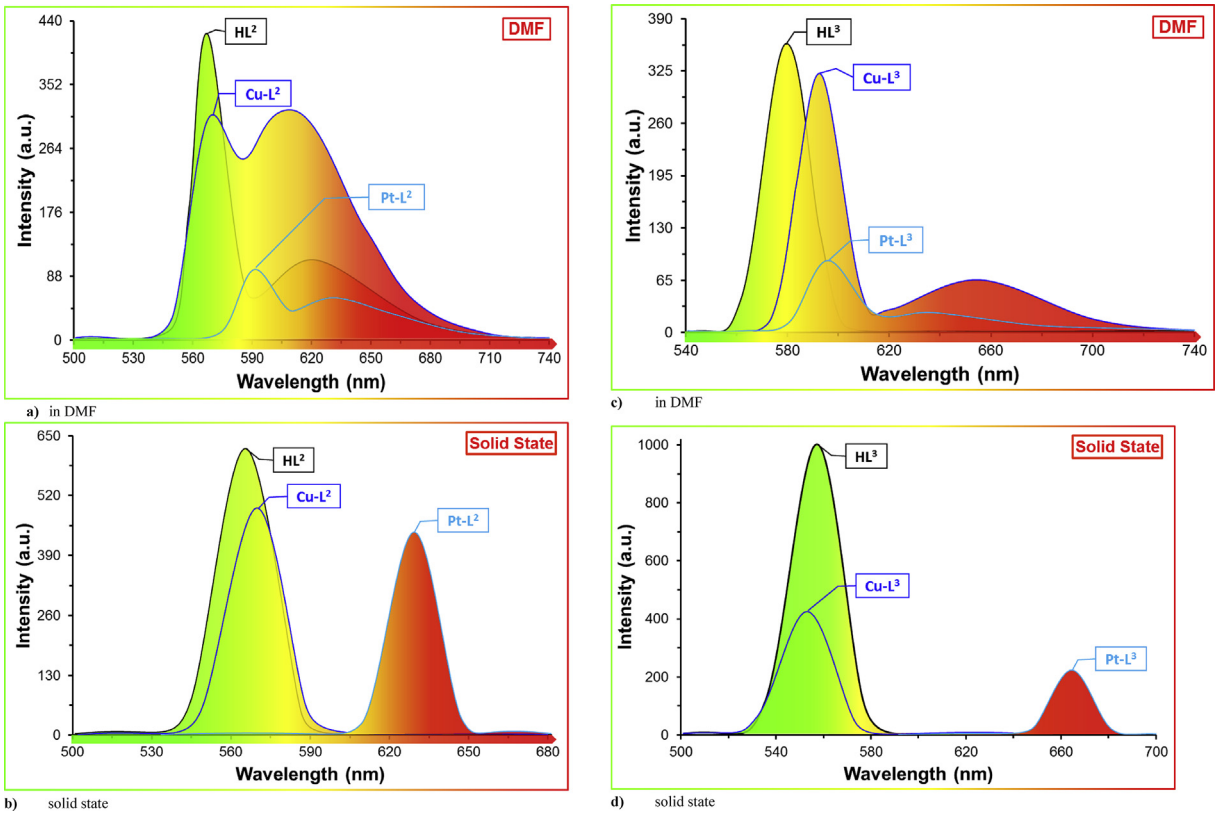

Fig. 4. The emission spectra of the HL^2 and HL^3 and their metal complexes in the DMF solution and solvent free (solid state).

complexes) have shifted to the longer wavelengths (red shift) [20,21]. The complexation of the ligands with Cu^{2+} or Pt^{2+} have caused a quenching in the emission bands due to the excited state energy transfer.

The CIE coordinates of the free ligands and their metal complexes in the DMF solution and solvent free media were calculated by using the PL spectral data given in Table 1. The CIE 1931 color space chromaticity diagrams of all compounds have depicted in Fig. 5. The colors of the compounds in DMF solution have changed from the orange to the purple. The x, y chromaticity values of the complexes are bigger than free ligands. In the solvent free media, the free ligands and their Cu^{2+} and Pt^{2+} metal complexes have the major x, y chromaticity coordinates. As seen from Fig. 5, the chromaticity coordinates of all compounds (x:0.7471 and y:0.3512) are close to National Television Standard Committee (NTSC) standard CIE values for red color (x: 0.670, y:0.330) [22].

3.3. Electrochemical properties of the ligands and their metal complexes

The redox behaviours of the free ligands and their complexes (Cu^{2+} and Pt^{2+}) have been studied by using the cyclic voltammetry

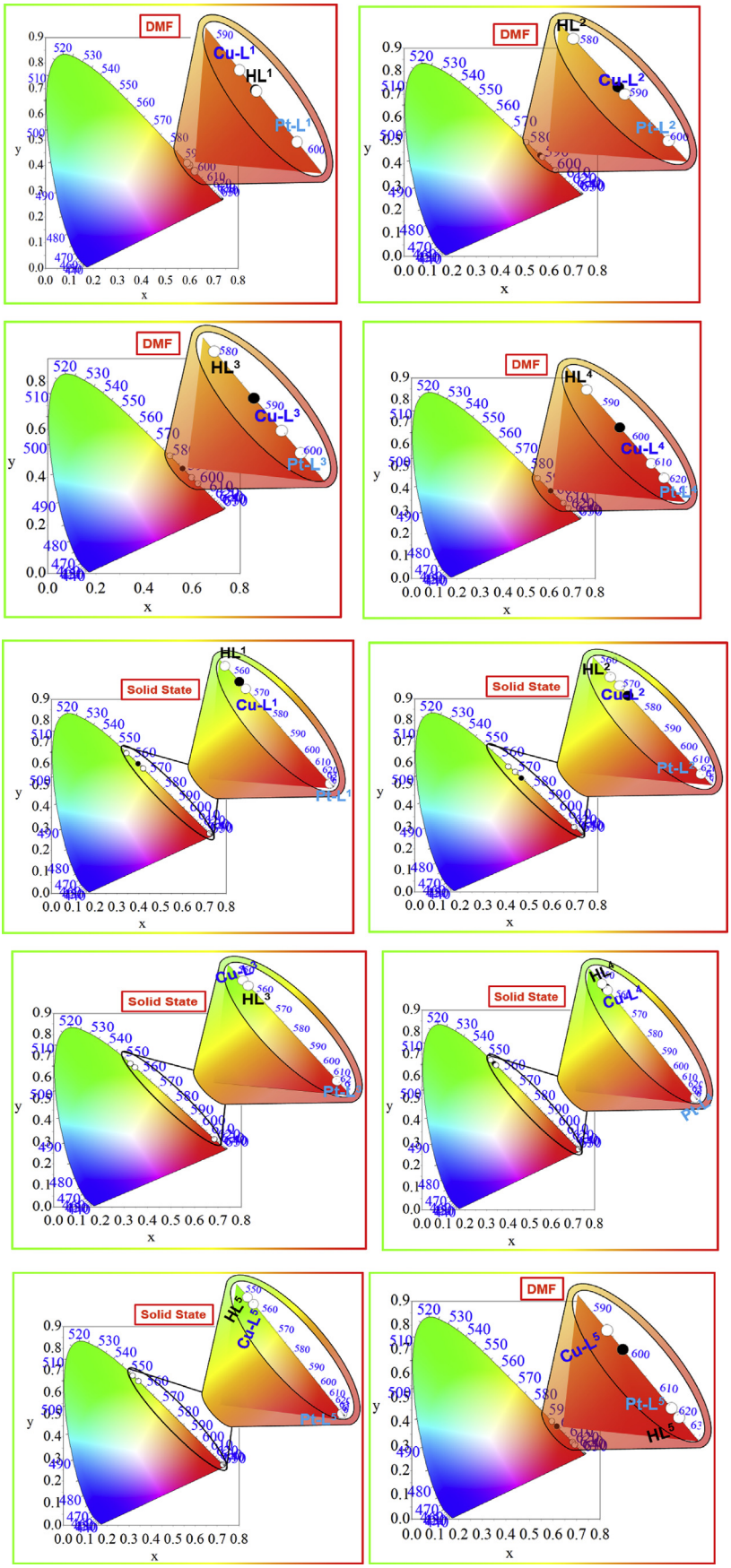

Fig. 5. Commission Internacionale d'Eclairage (CIE) coordinates for the ligands and their Cu(II) and Pt(II) complexes.

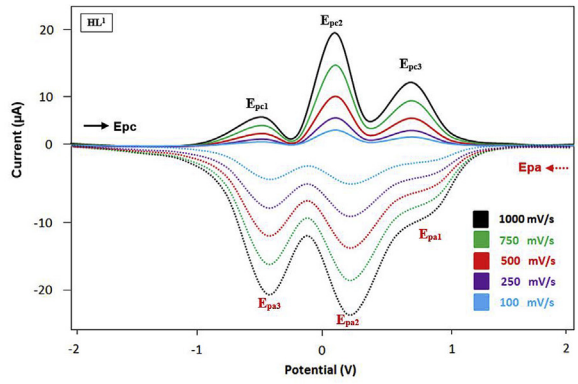

a) HL^1

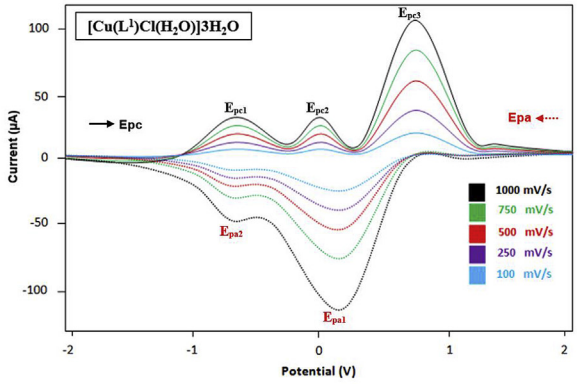

c) $[Cu(L^1)Cl(H_2O)]3H_2O$

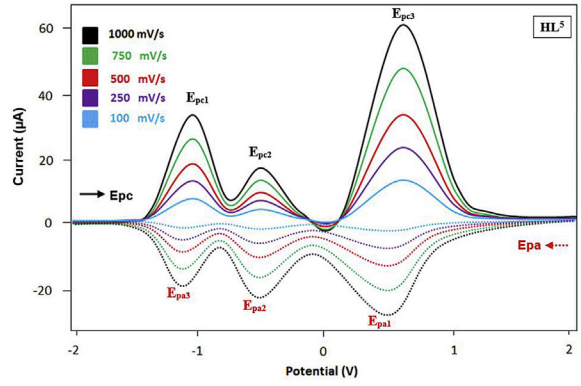

b) HL^5

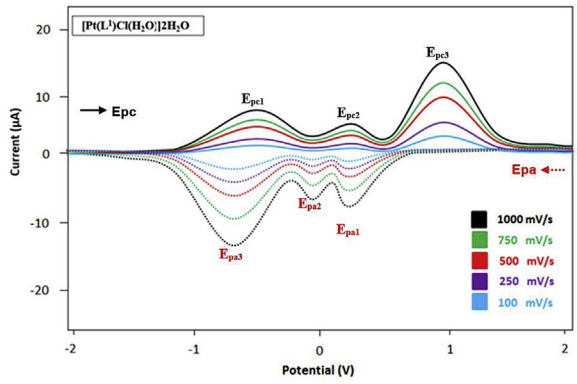

a) $[Pt(L^1)Cl(H_2O)]2H_2O$

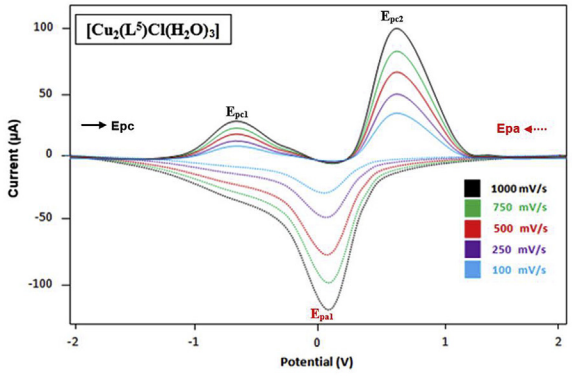

d) $[Cu_2(L^5)Cl(H_2O)_3]$

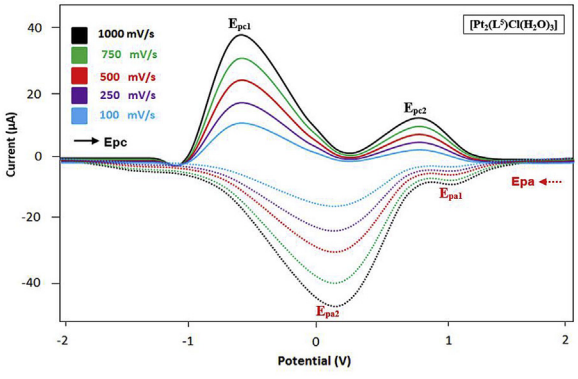

a) $[Pt_2(L^5)Cl(H_2O)_3]$

Fig. 6. a-f. The cyclic voltammograms of the azo-imine compound HL^1, HL^5 and their Cu^{2+} and Pt^{2+} complexes in the scan rate 100–1000 $mVsn^{-1}$ and 1.0×10^{-5} M DMF solution.

in 1.0×10^{-5} M DMF (0.1 M Bu_4NBF_4 as supporting electrolyte) at room temperature. All potentials quoted refer to measurements run at a scan rates in the 100–1000 mVs^{-1} range and against an internal ferrocene–ferrocenium standard, unless otherwise stated. The obtained data have given in Supplemantary file. The cyclic curves of the compounds HL^1, HL^5, $[Cu(L^1)Cl(H_2O)]3H_2O$, $[Pt(L^1)Cl(H_2O)]2H_2O$, $Cu_2(L^5)Cl(H_2O)_3$ and $Pt_2(L^5)Cl(H_2O)_3$ have given in Fig. 6. Furthermore, the voltammograms of the $CuCl_2 \cdot 2H_2O$, K_2PtCl_4 and Bu_4NBF_4 and variation of peak currents with potential scan rate for the ligands and their metal complexes have been given in the Supplementary file as S1 and S2, respectively. In the cyclic voltammogram of the K_2PtCl_4, there are two anodic (E_{pa}) peak potentials at 0.08 and −0.58 V and one cathodic (E_{pc}) peak at −0.56 V, respectively. The $CuCl_2 \cdot 2H_2O$ salt shows one cathodic peak at 0.72 V and three anodic peaks at 1.0, 0.16 and −0.68 V. When the electrochemical values of the salts $CuCl_2 \cdot 2H_2O$ and K_2PtCl_4 are compared, it is seen that the anodic and cathodic peak potential values of the $CuCl_2 \cdot 2H_2O$ salt shift to more positive and negative

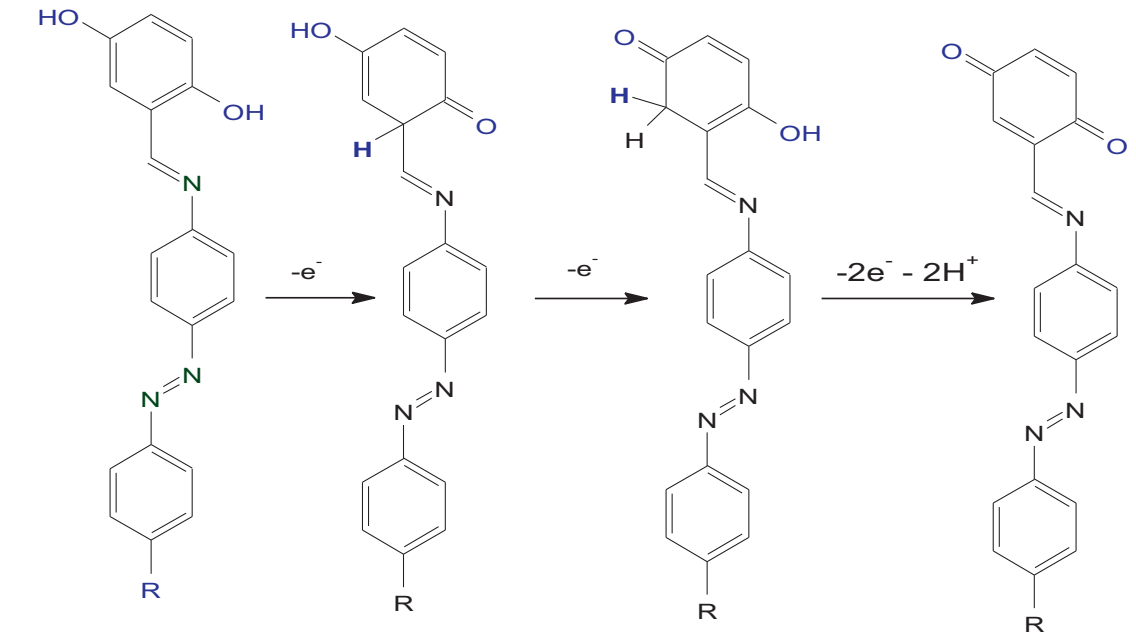

a) HL^3

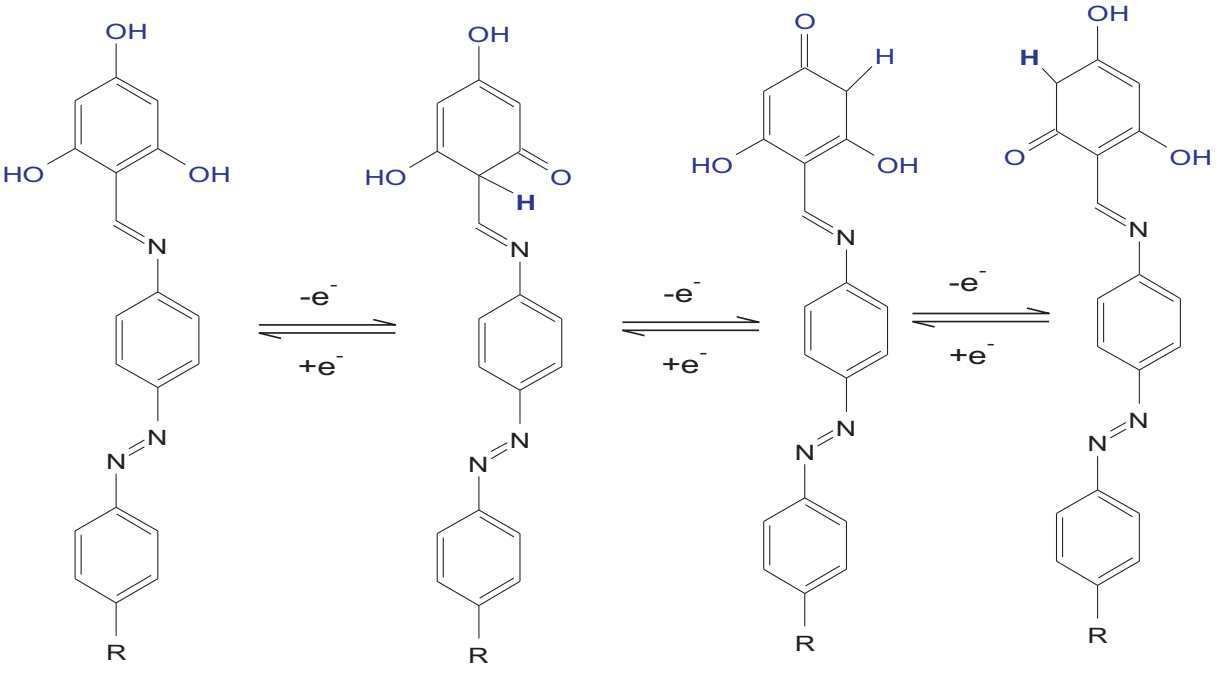

b) HL^5

Fig. 7. The proposed redox mechanisms for the ligands HL^3 and HL^5.

regions. On the other hand, the buffer (Bu_4NBF_4) has not any peak potential in the −2.0-(+)2.0 V range. The voltammograms of the ligands HL^1-HL^5 show the different redox processes in this range. The ligands HL^1, HL^3 and HL^5 have both anodic and cathodic peak couples in the −1.15-0.86 and −1.07−0.90 V, respectively. When the anodic and cathodic peak potential values of these ligands were compared, the E_{pc1} and E_{pa3} values of the ligand HL^5 have been shifted to the more negative regions than the ligands HL^1 and HL^3. This may be due to the position of the substituted groups attached to the salicylidene ring. While the ligand HL^3 at all scan rates shows the irreversible redox processes (Fig. 7a), the ligands HL^1 and HL^5 indicate the fully reversible reaction (Fig. 7b). In the proposed redox mechanism of the ligand HL^3, the first and second oxidation steps show a process with one electron. The last step indicates the irreversible oxidation process with two-electron. On the other hand, the metal free ligand HL^5 shows exactly three reversible redox processes in the −1.15−0.65 V (E_{pa}/E_{pc}) and 100-1000 mVs^{-1} scan rate range. In all reversible processes (Fig. 7b) for ligand HL^5, all redox events correspond to a single electron. The redox properties of the ligand HL^1 are similar to the ligand HL^5. It is also reversible redox events at all scan rates. The ligands HL^2 and HL^5 show the similar electrochemical properties. That is, they have two anodic and two cathodic redox couples in the −0.48-0.31 and −0.98-0.93 V, respectively. In these ligands, all redox processes are irreversible with one electron.

When the electrochemical properties of metal complexes are examined, it was determined that some complexes exhibited different electrochemical properties than ligands. The Pt^{2+} complexes of the HL^1 and HL^3 ligand has three cathodic and three anodic peak potentials in the −0.51-1.05 and −0.73−0.94 V range, respectively. In these complexes, all redox processes are irreversible. The other Pt^{2+} complexes have also different numbers E_{pa} and E_{pc} values. The redox processes in all Pt^{2+} complexes are irreversible. The redox event in some of the Pt^{2+} complexes is ligand centered and some are metal centered. On the other hand, the Cu^{2+} complexes of the HL^2, HL^4 and HL^5 ligands have two cathodic and one anodic peaks in the −0.70-0.99 and −0.14-0.09 V, respectively. While the Cu^{2+} complex of the ligand HL^1 shows three cathodic and two anodic peak potentials, the $[Cu(L^3)Cl(H_2O)]3H_2O$ complex show two anodic and two cathodic peak potentials. In the copper complexes, the redox processes are irreversible and ligand centered.

Cyclic voltammograms of HL^1, HL^5, $[Cu(L^1)Cl(H_2O)]3H_2O$, $[Pt(L^1)Cl(H_2O)]2H_2O$, $Cu_2(L^5)Cl(H_2O)_3$ and $Pt_2(L^5)Cl(H_2O)_3$ at various scan rates such as 100, 250, 500, 750 and 1000 mVs^{-1} were also recorded as shown in Fig. 6. It is found that both cathodic and anodic peak current linearly increases with the increasing of scan rate. The position of the cathodic peak slightly shifted towards the negative potential and the anodic peak shifted a little towards positive direction with the increase of scan rate. When the scan rate was increased, a linear relationship between the peak current and the scan rate in the range of 100−1000 mV/s was found (Fig. S2), suggesting an adsorption behaviour [23]. The equation relating to anodic current peak can be represented as:

$$I_{pa}(\mu A) = 536.92v(V/s) + 35.363, R_2 = 0.98$$

Thermal decomposing behaviours of the metal free ligands and their Cu^{2+} and Pt^{2+} complexes have investigated by using thermogravimetric (TGA) and differantial thermal analyses (DTA) methods in the 30−1000 °C temperature range. The TGA curves of the ligands have given in Fig. 8. The thermal decomposing behaviours of the metal free ligands are the similar. The thermal degradation of the ligands starts at the 224 °C and they lost most of their mass up to 420 °C temperature. At the 515 °C temperature, the

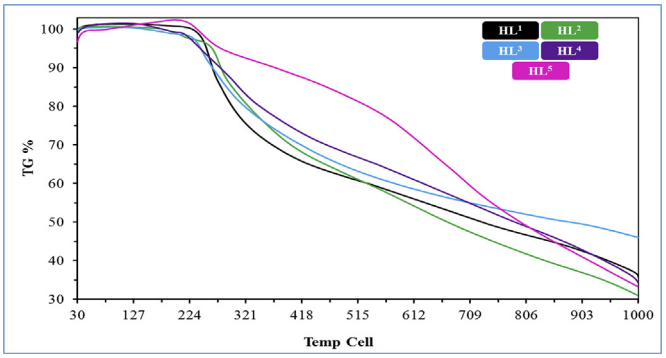

Fig. 8. Thermogravimetric curves (TGA) of the ligands HL^1-HL^5 in the 30−1000 °C temperature range.

second degradation process starts and continues to the 600 °C. The ligand HL^5 has more rmal stability than the other ligands. In the TGA curves of the Cu^{2+} and Pt^{2+} complexes, thermal degradation starts by lost the adsorbed water molecules in the 45−80 °C temperature range. At the higher temperatures (in the 125−250 °C temperature range), the water molecule and chlorine ion coordinated to the metal cations have lost from the complexes. Degradation of the organic part in the complexes begins in the 354−360 °C temperature range and the decomposition continues up to about 700 °C temperatures. Final degradation product of the metal complexes is the metal oxide (CuO or PtO). Compared to the thermal stability of metal complexes, the Pt^{2+} complexes have higher thermal stabilities than the Cu^{2+} complexes.

3.4. Dyeing applications on the wool by the metal free ligands and their metal complexes

Dye baths were prepared using 0.1−0.05 g dye in 35 mL distilled water. The images (after five times washing with soap) obtained after dyeing were given in Fig. 9. Moreover, the images after ten times washing and without mordants have been given in the Supplementary file as Fig. S1. Firstly, the DB9 has used in dyeing of the wool. During the dyeing process, mordanting reagents were added to the dye bath. The dyeing properties of the DB9, HL^1 and its Cu(II) and Pt(II) complexes on wool were studied without using mordanting agents and the color of the wools are given in Fig. S3. DB9 gave an intense orange color and the intensity of the color is almost retained even after ten times washing. It was determined that the DB9 dyed well the wool in the presence of all the used mordanting reagents. Conversely, the metal free ligand HL^1 was dyed the wool in the presence of the $FeSO_4$ and $Al_2(SO_4)_3$ mordanting agents. While the Cu^{2+} complex of the HL^1 ligand has excellent dyeing properties in the existence of the $K_2Cr_2O_7$, $FeCl_3$ and $FeSO_4$, the Pt^{2+} complex has best dyed the wool in the presence of the $K_2Cr_2O_7$, $FeCl_3$, $FeSO_4$ and $Al_2(SO_4)_3$ mordanting agents. The washing fastnesses of all compounds were investigated and after the ten washes, the colors of the dyed wools were slightly lighter. For the dyeing properties of DB9 and its derivatives, we proposed a mechanism in which the hydrophilic edges (ethylene hydroxy groups) of the dye molecules involve in ionic interactions with the amino groups of the wool as shown in Fig. 10.

4. Conclusion

In this study, five ligands and their Cu^{2+} and Pt^{2+} complexes have synthesized and characterized by the instrumental methods. The metal free ligands have three aromatic rings and these rings are conjugated with each other. Throughout the molecules, the π-

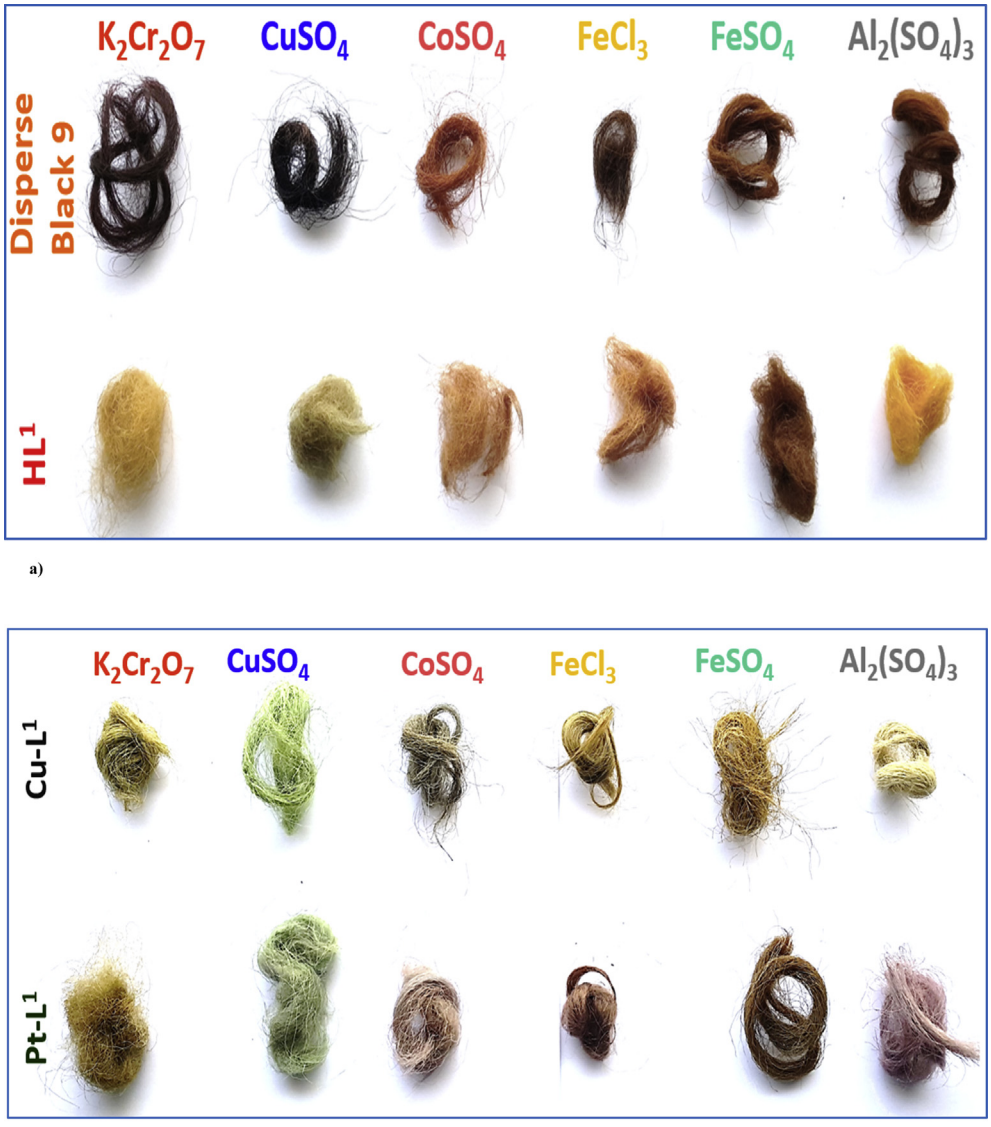

Fig. 9. a, b) Dyeing of wool with the disperse black 9, HL^1, $[Cu(L^1)Cl(H_2O)]3H_2O$ and $[Pt(L^1)Cl(H_2O)_2]2H_2O$ in water.

electrons of the aromatic rings are delocalized. Moreover, as there are the hydoxy groups on the salicylidene rings, these groups also donate the π-electrons by mesomeric effect to the aromatic rings. The anodic and cathodic peak potential values of the Pt^{2+} complexes have shifted to the more positive regions than the Cu^{2+} complexes. It can be said that platinum complexes are more difficult to reduce or oxidize than copper complexes (metal effect). The ligand HL^5 has more rmal stability than the other ligands. Compared to the thermal stability of metal complexes, the Pt^{2+} complexes have higher thermal stabilities than the Cu^{2+} complexes.

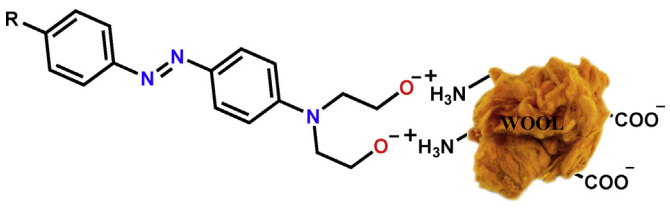

Fig. 10. The ionic interaction between dye molecules and amino groups of wool.

Acknowledgments

We are grateful to The Scientific & Technological Research Council of Turkey (TUBITAK) (Project number: 115Z065) for the support of this research.

Appendix A. Supplementary data

Supplementary data to this article can be found online at https://doi.org/10.1016/j.molstruc.2019.127135.

References

[1] L. Wang, Y. Hou, X. Zhong, J. Hu, F. Shi, Preparation and catalytic performance of alginate-based Schiff Base, Carbohydr. Polym. 208 (2019) 42–49.
[2] Ö. Özdemir, Synthesis and characterization of a new diimine Schiff base and its Cu^{2+} and Fe^{3+} complexes: investigation of their photoluminescence, conductance, spectrophotometric and sensor behaviors, J. Mol. Struct. 1179

(2019) 376–389.
[3] M. Ramesh, G. Venkatachalam, Half–Sandwich (η6–p–Cymene) Ruthenium(II) complexes bearing 5– Amino–1–Methyl–3–Phenylpyrazole Schiff base ligands: synthesis, structure and catalytic transfer hydrogenation of ketones, J. Organomet. Chem. 880 (2019) 47–55.
[4] D.S. Timofeeva, A.R. Ofial, H. Mayr, Nucleophilic reactivities of Schiff base derivatives of amino acids, Tetrahedron 75 (2019) 459–463.
[5] A. Palanimurugan, A. Kulandaisamy, DNA, in vitro antimicrobial/anticancer activities and biocidal based statistical analysis of Schiff base metal complexes derived from salicylalidene-4-imino-2,3-dimethyl-1-phenyl-3-pyrazolin-5-one and 2-aminothiazole, J. Organomet. Chem. 861 (2018) 263–274.
[6] S.S. Jawoor, S.A. Patil, S.S. Toragalmath, Synthesis and characterization of heteroleptic Schiff base transition metal complexes: a study of anticancer, antimicrobial, DNA cleavage and anti-TB activity, J. Coord. Chem. 71 (2) (2018) 271–283.
[7] V.R. Solomona, W. Haqa, M. Smilksteinb, K. Srivastavac, S. Rajakumar, S.K. Puric, S.B. Katti, Synthesis and antimalarial activity of novel side chain modified antimalarial agents derived from 4-aminoquinoline, Med. Chem. 4 (2008) 446–456.
[8] M. Sarkheil, M. Lashanizadegan, M. Ghiasi, High catalytic activity of magnetic Fe_3O_4@SiO_2-Schiff base-Co(II) nanocatalyst for aerobic oxidation of alkenes and alcohols and DFT study, J. Mol. Struct. 1179 (2019) 278–288.
[9] A. Bilgin, S. Çetintaş, E. Cerrahoğlu, U. Yıldız, D. Bingöl, A new Schiff base: synthesis, characterization and optimization of metal ions-binding properties, Separ. Sci. Technol. 51 (13) (2016) 2138–2144.
[10] S.A. Güngor, M. Köse, F. Tümer, M. Tümer, Photoluminescence, electrochemical, SOD activity and selective chemosensor properties of novel asymmetric porphyrin-Schiff base compounds, Dyes Pigments 130 (2016) 37–53.
[11] M. Tümer, F. Tümer, M. Köse, S.A. Gungor, S. Akar, İ. Demirtaş, G. Ceyhan, Structural characterizations, photophysical and biological properties of Disperse black 9 dye and π-extended imine derivatives, Dyes Pigments 154 (2018) 62–74.
[12] S. Özkınalı, M. Gür, N. Şener, S. Alkın, M.S. Çavuş, Synthesis of new azo schiff bases of pyrazole derivatives and their spectroscopic and theoretical investigations, J. Mol. Struct. 1174 (2018) 74–83.
[13] R. Arabahmadi, M. Orojloob, S. Amani, Azo Schiff bases as colorimetric and fluorescent sensors for recognition of F^-, Cd^{2+} and Hg^{2+} ions, Anal. Methods 6 (2014) 7384–7393.
[14] B.T. Thaker, J.B. Kanojiya, R.S. Tandel, Effects of different terminal substituents on the mesomorphic behavior of some azo-schiff base and azo-ester-based liquid crystals, Mol. Cryst. Liq. Cryst. 528 (2010) 120–137.
[15] M. Jalali-Heravi, A.A. Khandar, I. Sheikshoaie, A theoretical investigation of the structure, electronic properties and second-order nonlinearity of some azo Schiff base ligands and their monoanions, Spectrochim. Acta, Part A 55 (1999) 2537–2544.
[16] N.N. Ayare, S.H. Ramugade, N. Sekar, Photostable coumarin containing azo dyes with multifunctional property, Dyes Pigments 163 (2019) 692–699.
[17] C.H. dos Santos, N.M. Uchiyama, I.A. Bagatin, Selective azo dye-based colorimetric chemosensor for F^-, CH_3COO^- and PO_4^{3-}, Spectrochim. Acta, Part A 210 (2019) 355–361.
[18] J. Qiu, J. Xiao, B. Tang, B. Ju, S. Zhang, Facile synthesis of novel disperse azo dyes with aromatic hydroxyl group, Dyes Pigments 160 (2019) 524–529.
[19] F. Tümer, M. Köse, S. Akar, S.A. Güngör, M. Tümer, Structural characterization of disperse black 9 based Cu (II) complex and investigation of its some properties, Appl. Organomet. Chem. e4764 (2019) 1–9.
[20] S. Tirapattur, M. Belletête, N. Drolet, J. Bouchard, M. Ranger, M. Leclerc, G. Durocher, Spectroscopic study of intermolecular interactions in various oligofluorenes: precursors of light-emitting polymers, J. Phys. Chem. B 106 (2002) 8959–8966.
[21] F.D. Lewis, J.S. Yang, Solid-state fluorescence of aromatic dicarboxamides. Dependence upon crystal packing, J. Phys. Chem. B 101 (1997) 1775–1781.
[22] G. Shao, H. Yu, N. Zhang, Y. He, K. Feng, X. Yang, R. Cao, M. Gonga, Synthesis and photophysical properties of europium(III)eb-diketonate complexes applied in LEDs, Phys. Chem. Chem. Phys. 16 (2) (2014) 695–702.
[23] A.J. Bard, L.R. Faulkner, Electrochemical Methods, Fundamentals and Applications, John Wiley & Sons Inc., New York, 2001.